Paper Submitted to the 83rd TRB

Anisotropic Properties of Asphalt Concrete: Characterization and Implications in Pavement Design and Analysis

Dr. L.B.Wang, Assistant Professor (Contact Author)
Department of Civil and Environmental Engineering
Louisiana State University and Southern University
Baton Rouge, LA 70803
Tel: (225)578-4821
Fax: (225)578-8652
Email:lwang@lsu.edu

Dr. Laureano R. Hoyos, Assistant Professor,
Department of Civil Engineering
University of Texas at Arlington
Arlington, TX 76019

Dr. Jay Wang, Assistant Professor
Department of Civil Engineering,
Louisiana Tech University
Ruston LA 71272

Dr. George Voyiadjis, Professor
Department of Civil and Environmental Engineering
Louisiana State University
Baton Rouge, LA 70803

Mr. Chris Abadie, P.E., Materials Research Administrator
Louisiana Transportation Research Center
Baton Rouge, LA 70803

January 2004
Washington, DC

Anisotropic Properties of Asphalt Concrete: Characterization and Implications in Pavement Design and Analysis

Linbing Wang[1], Laureano R. Hoyos[2], Jay Wang[3], George Voyiadjis[4] and Chris Abadie[5]

ABSTRACT

Asphalt concrete has been recognized as an anisotropic material. However the degree of anisotropy and its implications in pavement design and analysis have not been well understood. This paper illustrates the difference of the stress field between an isotropic and an anisotropic pavement under wheel load through analytical solution and Finite Element simulation. A servo-controlled true triaxial (cubical) testing device was used to test four-inch cubical asphalt concrete specimens under general stress states to characterize the anisotropic properties of asphalt concrete. It was discovered that: a) the stiffness of cored field specimen has significant difference in vertical and horizontal direction; b) the significant difference may result in larger shear stress and tensile stress in a pavement. These findings indicate that characterization and modeling of the anisotropic properties of asphalt concrete is an important area that deserves further investigations.

INTRODUCTION

Asphalt concrete is a bonded granular material. Its internal structure is anisotropic, which could be due to the anisotropic particle and void shape, particle orientation distribution, and anisotropic compaction (restrain and force pattern applied during the compaction). The characterization and modeling of the anisotropic properties of soils have been widely explored in geomechanics and

[1] Assistant Professor, Department of Civil and Environmental Engineering, Louisiana State University and Southern University, Baton Rouge, LA 70803
[2] Assistant Professor, Department of Civil and Environmental Engineering, University of Texas at Arlington, Arlington, TX 76019
[3] Assistant Professor, Department of Civil Engineering, Louisiana Tech University, Ruston LA 71272
[4] Professor, Department of Civil and Environmental Engineering, Louisiana State University and Southern University, Baton Rouge, LA 70803
[5] Materials Research Administrator, Louisiana Transportation Research Center, Baton Rouge, LA 70803

geotechnical engineering [1,2,3,4,5]. However, few studies have focused on the characterization and modeling of aggregate base [6,7], asphalt concrete [8] and pavement analysis [9]. It would be worthwhile that the degree of anisotropy and its effect on material response could be evaluated because the characterization and analysis methods for isotropic and anisotropic materials are quite different. In general, whether a material is isotropic or anisotropic affects the selection of materials characterization methods, response models and distress models. For example, if the axial stiffness and the lateral stiffness of a gyratory specimen are significantly different from those of a field specimen, the deformation characteristics obtained using gyratory specimens may not well represent those of field specimens. This paper presents a comparison between the stress field of an isotropic and anisotropic pavement through an analytical solution and Finite Element (FE) simulations, and a method to characterize the orthotropic material properties using a Cubical device.

ANISOTROPIC ELASTICITY AND ITS IMPLICATION

Orthotropic Elasticity

Asphalt concrete is a viscoplastic material. In pavement analysis and especially stress analysis it is often treated as an isotropic elastic material. This treatment has its advantage in simplicity. It has also some theoretical basis in that the initial stresses at t=0 have significant influence on the subsequent viscous and plastic deformation and the stress analysis can be performed using elasticity theory through the elastic-viscoelastic correspondence principle. In this study, an anistropic elasticity analysis of a pavement under wheel load is presented. Although asphalt concrete may demonstrate the general anisotropy, only cross anisotropy or orthotropy is considered in this study for simplification purposes, and some experimental evidence presented

in the experimental section of this paper. In the orthotropic case, asphalt concrete is considered to have significant difference only in vertical and horizontal directions due to the anisotropic compaction, restrain conditions and gravity direction. In orthotropic elasticity, there are only five material constants. However, the general anisotropic elasticity has 21 materials constants and is not realistic for modeling and characterization. The five materials constants of the orthotropic elasticity are $E_v, E_h, \nu_{vh}, \nu_{hh}$ and G_{vh}. Where E_v and E_h are elastic modulus in vertical and horizontal directions respectively; ν_{vh} and ν_{hh} are Poisson's ratios for vertical-horizontal and horizontal-horizontal responses respectively; and G_{vh} is the shear modulus along the vertical plane. The Hooke's Law for the orthosotropic case can be expressed as follows:

$$\Delta\varepsilon_x = \frac{1}{E_h}\Delta\sigma_x - \nu_{hh}\frac{1}{E_h}\Delta\sigma_y - \nu_{vh}\frac{1}{E_v}\Delta\sigma_z \qquad (1a)$$

$$\Delta\varepsilon_y = \frac{1}{E_h}\Delta\sigma_y - \nu_{hh}\frac{1}{E_h}\Delta\sigma_x - \nu_{vh}\frac{1}{E_v}\Delta\sigma_z \qquad (1b)$$

$$\Delta\varepsilon_z = \frac{1}{E_v}\Delta\sigma_y - \nu_{vh}\frac{1}{E_h}\Delta\sigma_x - \nu_{vh}\frac{1}{E_v}\Delta\sigma_y \qquad (1c)$$

$$\Delta\gamma_{yz} = \frac{1}{G_{vh}}\Delta\tau_{yz} \qquad (1d)$$

$$\Delta\gamma_{zx} = \frac{1}{G_{vh}}\Delta\tau_{zx} \qquad (1e)$$

$$\Delta\gamma_{xy} = \frac{(1+\nu_{hh})}{E_h}\Delta\tau_{xy} \qquad (1f)$$

where $\Delta\varepsilon_x, \Delta\varepsilon_y, \Delta\varepsilon_z$ are normal strain increments and $\Delta\sigma_x, \Delta\sigma_y, \Delta\sigma_z$ are normal stress increments; $\Delta\gamma_{yz}$ $\Delta\gamma_{yz}$ $\Delta\gamma_{xy}$ are shear strain increments; and $\Delta\tau_{yz}$ $\Delta\tau_{zx}$ $\Delta\tau_{xy}$ the corresponding shear strain increments.

Boussinesq's Solution for Orthotropic Materials

For a full-depth asphalt concrete pavement (isotropic materials), if the distributed tire load could be approximated as a central load, the stress field could be approximated by the Boussinesq's solution, a half-space subjected to a concentrated load *P* as illustrated in Figure 1. The corresponding Boussinesq's solution for orthotropic material was obtained by Wolf [10]. The analytical expressions for two of the four stress components, σ_θ and τ_{rz}, are presented in equations (2) and (3). The solution is based on the cylindrical coordinate system shown in Figure 1. The parameters $s_1, s_2, a, c, d, q_1, q_2, \lambda, \mu$ are related to $E_v, E_h, \nu_{vh}, \nu_{hh}, G_{vh}$. Their implications can be found in [10].

$$\sigma_\theta = -\frac{P}{2\pi}\{\frac{\sqrt{d}}{ac-d}\frac{z}{s_1-s_2}[-\frac{s_1^2 q_2}{(r^2+s_1^2 z^2)^{3/2}}+\frac{s_2^2 q_1}{(r^2+s_2^2 z^2)^{3/2}}]-\frac{\lambda}{s_1-s_2}\frac{z}{r^2}[\frac{s_1^2 p_2}{(r^2+s_1^2 z^2)^{3/2}}-\frac{s_2^2 p_1}{(r^2+s_2^2 z^2)^{3/2}}]$$

$$+\frac{\mu}{r^2}\} \qquad (2)$$

$$\tau_\theta = -\frac{P}{2\pi\sqrt{d}}\frac{z}{s_1-s_2}[\frac{1}{(r^2+s_1^2 z^2)^{3/2}}-\frac{1}{(r^2+s_2^2 z^2)}] \qquad (3)$$

To illustrate how these two stress distributions vary with the elastic materials constants, the solutions for σ_θ and τ_θ are plotted in Figures 2a and 2b for $E_h = 1.0, 0.9, 0.7, 0.5, 0.2E_v, \nu_{vh} = \nu_{hh} = 0.3$, and G_{vh}=0.384E_h (see the experimental data in the experiment section). It can be seen that both stresses are larger than those of the isotropic cases if horizontal stiffness is smaller than the vertical stiffness (see the experimental data for the justification). This fact has an important implication for pavement design and analysis. The

larger tensile stress σ_θ may imply that the fatigue cracking stress level might be underestimated by using isotropic elasticity stress analysis; the larger shear stress τ_θ may imply that shear flow is underestimated using the isotropic elasticity stress analysis.

FEM Analysis of a Model Pavement

The above solution refers to the half-space case or to the full-depth asphalt pavement case. For the layered pavement, a FEM analysis is needed (a commercial software ADINA is used in this study). In the FEM analysis, a block of asphalt concrete of $5\times5\times3$ in^3 subjected to a 100 lb load distributed on a 0.5 inch strip is simulated. The block is discretized into 1000 3-D 20-node solid elements. Two sets of boundary conditions are applied. In set one, the bottom surface is fixed in X, Y and Z directions (see Figure 3); all the other 4 lateral surfaces are fixed in normal directions (horizontal directions). In set two, the bottom surface is fixed in Z directions only and all the other 4 lateral surfaces are fixed in normal directions (horizontal directions). This configuration is similar to the testing configuration of the Asphalt Pavement Analyzer (APA). Use of this setup has an objective for future study using APA. As linear elasticity is involved, the configuration can be proportionally scaled to larger sections. Table 1presents the materials inputs for the simulation. The simulation mainly evaluates how the ratio between horizontal and vertical stiffness affects the stress distribution and vertical displacements. The analysis is performed for five elastic modulus ratios (E_h/E_v=1,0.8, 0.5, 0.2, 0.1).

Figures 3 and 4 present the comparisons of stresses and displacements at elastic modulus ratio of 0.2 for set one and set two boundary conditions respectively. Other cases are similar and the general trend is that the more significant of the anisotropy the larger the differences in stress and displacement fields. Analysis of the data presented in figures 3 and 4 and other cases indicates that under the above boundary conditions and materials properties, the largest effective stress

(the von Mises stress) and the vertical displacement increases with the increase of anisotropy; the largest tensile stress in yy direction decreases with the increase of anisotropy. It should be noted that the horizontal stiffness (in y direction) decreases with the increase of anisotropy and therefore the tensile stresses decrease (the normal direction is restrained).

Although a definitive conclusion (i.e. increase or decrease, safe or unsafe) about the trend due to the effects from anisotropy cannot be drawn based on this limited study, the analysis indeed indicates some significant differences. Further study to characterize the materials constants and to apply rational boundary conditions is needed.

CHARACTERIZATION OF THE ANISOTROPIC PROPERTIES USING TRUE TRIAXIAL (CUBICAL) TESTING DEVICE

General

Even though different types of true triaxial devices have been developed worldwide, they can be classified into three categories: (1) Rigid boundary type [11, 12], (2) Flexible boundary type [13, 14], and (3) Mixed boundary type [15, 16]. The advantages and disadvantages of these three types of true triaxial devices have been discussed by Sture [17] and Arthur [18]. The original development of the flexible boundary type of device used in this work was presented by Atkinson [19] for multiaxial testing of rock materials. A detailed description of the original components is presented by Atkinson [19], Sture [17], and NeSmith [20]. The stress-controlled, computer-driven cubical testing device consists basically of six main components or modules: (1) A frame, (2) Six wall assemblies, (3) A deformation measuring system, (4) A stress application and control system, (5) Six rigid membranes, and (6) A data acquisition and process control system (DA/PCS). A detailed, illustrated description of these components follows.

The Cubical Device System

Steel frame

A photograph of the true triaxial cubical frame is shown in Figure 5a. The frame supports the top and four lateral wall assemblies, the cubical asphalt concrete specimen, and the bottom wall assembly. An inner square cavity was machined into each of the six faces of the frame to accommodate the membranes and to form the pressure cavities. Connection bolts were provided on each face of the frame to fix the wall assemblies. The function of the frame is twofold: (1) It forms the top, bottom, and lateral sides of the six pressure chambers (wall assemblies) that apply the external multiaxial load to the cubical asphalt concrete specimen, and (2) It serves as the reaction structure for the application of the total normal stresses to the top, bottom, and lateral faces of the cubical asphalt concrete specimen. The frame was machined from a solid billet of AISI 4140 heat treated, re-sulfurized, forged steel. The outside of the frame was machined to a dimension of 23.0 cm (9.05 in), while the inner square cavities have a dimension of 10.35 cm (4.07 in). A 0.13 cm (0.05 in) radius is provided at the inner corners of the square cavities to reduce stress concentrations. The working pressure limits are 132.50 MPa (19200 psi) for uniaxial pressures, and 64.52 MPa (9350 psi) for a hydrostatic loading condition [19, 20].

Top, bottom, and lateral wall assemblies

Figures 5 b and c show a photograph of the wall assembly. The walls were machined from a 7075-T6 aluminum plate [19], and are fastened to the frame by steel studs mounted in tapped holes on the exterior of the frame. Each wall assembly consists mainly of three components: (1) A cover plate, which provides the wall seal for the interior pressure cavity, (2) Two threaded fluid pressure inlet/outlet connections, and (3) Three threaded holes to receive the stainless steel

housing of the LVDTs (linear variable differential transformers). When the membranes are mounted on the frame, each assembly provides an effective seal against the leaking of the pressurized fluid to the atmosphere. An O-ring groove on the wall forms the pressure seal between the wall assembly and the reaction frame.

Deformation measuring system

The deformation of the cubical asphalt concrete specimen is measured at three points on the top, bottom, and each of the four lateral faces, using 18 LVDTs (3 LVDTs/face). The core of each LVDT and its extension rod are thrust into contact with the rigid membranes by a low-stiffness spring (Figure 5). Two threaded locknuts were used as the tip of each LVDT's extension rod. A zinc-plated steel flat washer allows for complete extension or compression of the spring. The output from the LVDTs is recorded by means of a data acquisition and process control system (DA/PCS). The 499 XS-C's Schaevitz series, high-pressure sealed LVDT (from Lucas Control Systems Products, Inc.), is suitable for operating pressures up to 210 bars (3000 psi) in pressure-sealed chambers, with a nominal linear range of +/- 12.50 mm (+/- 0.50 in). The EB-welded stainless steel housing is highly resistant to corrosive environments, and its internal magnetic and electrostatic shielding render the XS-C's LVDT insensitive to external magnetic influences. The sampling rate during a test can be easily selected from the menu of a data acquisition and process control computer software (LABTECH-NOTEBOOK from Laboratory Technologies Corp.). The computer software allows for the real time display of the 18 LVDT channels. The analog input (Volt) signal delivered by the leadwires of the LVDTs is converted into a digital output signal by an analog-to-digital converter (RTI-815 board from Analog Devices, Inc.), plugged into the CPU of the PC-based computer. The deformation of each side of the specimen, along a particular direction, is estimated by averaging the three LVDTs' outputs corresponding to the specimen's

face, X(+/-), Y(+/-), or Z(+/-), perpendicular to that particular direction. The LVDTs are located at a 120^{o} spacing on a 3.18 cm (1.25 in) radius on each of the top and lateral wall assemblies.

Stress application and control system

The hydraulic pressure applied through the six rigid membranes to the top, bottom and lateral sides of the cubical asphalt concrete specimen, is generated and controlled by a computer-driven electro-hydraulic pressure system. The fluid is pressurized by a 20 gal. standard hydraulic power unit or pump (manufactured and installed by ORTON Industries, Inc.), that can deliver a variable output pressure up to 10.35 MPa (1500 psi) on each side of the specimen, depending on the initial setting and calibration of three computer-driven proportional pressure relief valves (manufactured by Parker Motion & Control, Inc.), connected to an equal number of outlet ports in the power unit (Figure 6). The RE series proportional relief valves provide for variable hydraulic pressure control in response to a variable voltage or current command signal. The RE series' valves feature an on-board electronic driver with adjustments for the rate at which the pressure increases and decreases (Figure 6). In addition, there are adjustments to electronically set the minimum pressure and maximum pressure delivered to the specimen (valves' calibration process). For this research study, the proportional pressure relief valves were calibrated to work at a minimum pressure of 175 kPa (25 psi), and a maximum pressure of 1225 kPa (175 psi). The output lines from the three proportional pressure relief valves split into two lines to supply the pressures to the positive (+) and negative (-) faces of the cubical asphalt concrete specimen for each particular loading condition. These positive and negative faces are designated as X(+), X(-), Y(+), Y(-), accounting for the four lateral sides, and Z(+), Z(-), accounting for the top and bottom sides. The output lines from the valves are transmitted to the test cell by flexible hoses having a rated burst strength of 27.50 MPa (4000 psi).

A quick-disconnect coupling between the hose and the fluid pressure inlet/outlet connections of the wall assembly makes for easy assembly. Any principal stress combination path can be achieved by simultaneous control over the three computer-driven proportional relief valves. The proportional relief valves receive an analog input (Volt) signal from an analog output signal-conditioning interface (IOB120-01 interface kit from Analog Devices, Inc.), connected to the digital-to-analog converter (RTI-815 board from Analog Devices, Inc.) plugged into the CPU of the computer. Low-viscosity Mobil-type (DTE 26) hydraulic fluid was used as the pressurizing medium.

Rigid membranes

Rigid membranes transmit the applied pressure uniformly to the top, bottom, and lateral faces of the cubical asphalt concrete specimen. They form the actual fluid barrier of the hydraulic fluid acting against the cubical asphalt concrete specimen. The membrane extends past the O-ring mounted in the inner face of the wall assemblies.

Data acquisition and process control system (DA/PCS)

An automated data acquisition and process control system (DA/PCS) was assembled to control the pressures applied to the cubical asphalt concrete specimen, and to monitor and record its resulting deformations. Details of this system are presented by NeSmith [20]. A photograph of the complete testing setup is shown in Figure 7.

Tests

To investigate the capability of the cubical cell device in evaluating the properties of asphalt concrete, a multistage loading procedure was adopted. Multistage loading runs different tests such as triaxial compression, triaxial extension and cyclic loading on the same specimen, eliminating the requirements on multiple specimens. This is especially useful when low-level

stress is involved, causing little or no damage. If numerical simulation can be used to account for specimen change, the results can be better interpreted.

A cubic specimen of 4-inch lateral length was cut from a block sample for the tests. The block sample is cored from the WesTrack project. The mix has targeted asphalt content of 5.7% and air void content of 8%. Loading procedure for the specimen is as follows: Isotropic Compression (IC) to 25 psi in each direction followed by Triaxial Compression (TC), Triaxial Extension (TE), Simple Shear (SS), Conventional Triaxial Compression (CTC), Conventional Trixaxial Extension (CTE), and cyclic CTE tests. Figures 8a and 8b present the loading sequences in $\sigma_x, \sigma_y, \sigma_z$ space and $\tau \sim p$ space respectively, where $\tau = \sqrt{(\sigma_x - \sigma_y)^2 + (\sigma_y - \sigma_z)^2 + (\sigma_z - \sigma_x)^2}$ $p = (\sigma_x + \sigma_y + \sigma_z)/3$. An initial stress of 25 psi is necessary to keep the membranes in good contact with the specimen. Stress paths for IC, TC, TE, SS, CTC and CTE tests were accomplished by simultaneous control of major, intermediate and minor principal stresses as follows:

Isotropic Compression (IC):

$$\Delta\sigma_x = \Delta\sigma_y = \Delta\sigma_z = \Delta\sigma$$

Triaxial Compression (TC):

$$\Delta\sigma_x = \Delta\sigma, \Delta\sigma_y = \Delta\sigma_z = -\frac{1}{2}\Delta\sigma \,, \Delta\sigma_y = \Delta\sigma, \Delta\sigma_x = \Delta\sigma_z = -\frac{1}{2}\Delta\sigma$$

$$\Delta\sigma_z = \Delta\sigma, \Delta\sigma_x = \Delta\sigma_y = -\frac{1}{2}\Delta\sigma$$

Triaxial Extension (TE):

$$\Delta\sigma_x = -\Delta\sigma, \Delta\sigma_y = \Delta\sigma_z = \frac{1}{2}\Delta\sigma \,, \Delta\sigma_y = -\Delta\sigma, \Delta\sigma_x = \Delta\sigma_z = \frac{1}{2}\Delta\sigma$$

$$\Delta\sigma_z = -\Delta\sigma, \Delta\sigma_x = \Delta\sigma_y = \frac{1}{2}\Delta\sigma$$

Simple Shear (SS)

$$\Delta\sigma_x = 0, \Delta\sigma_y = \Delta\sigma, \Delta\sigma_z = -\Delta\sigma \;\; \Delta\sigma_x = 0, \Delta\sigma_y = -\Delta\sigma, \Delta\sigma_z = \Delta\sigma$$

$$\Delta\sigma_y = 0, \Delta\sigma_x = \Delta\sigma, \Delta\sigma_z = -\Delta\sigma \;\; \Delta\sigma_y = 0, \Delta\sigma_x = -\Delta\sigma, \Delta\sigma_z = \Delta\sigma$$

$$\Delta\sigma_z = 0, \Delta\sigma_y = \Delta\sigma, \Delta\sigma_z = -\Delta\sigma \;\; \Delta\sigma_z = 0, \Delta\sigma_y = -\Delta\sigma, \Delta\sigma_z = \Delta\sigma$$

Conventional Triaxial Compression (CTC)

$$\Delta\sigma_x = \Delta\sigma, \Delta\sigma_y = 0, \Delta\sigma_z = 0 \;\; \Delta\sigma_x = 0, \Delta\sigma_y = \Delta\sigma, \Delta\sigma_z = 0$$

$$\Delta\sigma_y = 0, \Delta\sigma_x = 0, \Delta\sigma_z = \Delta\sigma$$

Conventional Triaxial Extension (CTE)

$$\Delta\sigma_x = -\Delta\sigma, \Delta\sigma_y = 0, \Delta\sigma_z = 0 \;\; \Delta\sigma_x = 0, \Delta\sigma_y = -\Delta\sigma, \Delta\sigma_z = 0$$

$$\Delta\sigma_y = 0, \Delta\sigma_x = 0, \Delta\sigma_z = -\Delta\sigma$$

Cyclic Conventional Triaxial Extension (CCTE):

The CTE test ran for a number of cycles.

Where $\Delta\sigma_x, \Delta\sigma_y, \Delta\sigma_z$ are load increments and $\Delta\sigma > 0$.

It should be noted that TC, TE and SS tests are run at *p=const* or on the π plane. The stress paths of these three tests in the principal stress space are illustrated in Figure 9. There are three variations for TC and TE stress paths respectively, and six variations for SS stress paths. Table 2 listed all the stress paths that were followed in the test.

Calculation of Modulus from Experimental Data

Since both stresses and strains in the three orthogonal orientations are monitored during each loading process, the information presented can be used to calibrate constitutive models. By eliminating the creeping strain (achieved using incremental stress and strain relations), the magnitudes of E_v, E_h can be calculated from CTC and CTE tests. Once E_v, E_h are obtained, ν_{vh}, ν_{hh} can be obtained from TC, TE or IC tests. G_{vh} can be obtained from the SS test that is involved with Z direction (for example, $\Delta\tau_{yz} = \Delta\sigma, \Delta\gamma_{yz} = \Delta\varepsilon_y - \Delta\varepsilon_z$ and using equation 1d). From the two tests performed, it was found that roughly E_{v}=200000 psi, E_{hh}=60000 psi, the Poisson's ratios ν_{vh}, ν_{hh} are 0.30, and G_{vh} =100000 psi. Figure 10 presents the IC test results; it can be seen that asphalt concrete compacted in the field follows a general anisotropy. The vertical modulus is usually 2~5 times' larger than the horizontal modulus. The test is performed at room temperature (20C). These relations are the basis for the FEM analysis. There are many other properties of asphalt concrete that can be characterized from the test. For example, Figure 11 presents the volumetric strain changes during the entire test while Figure 12 presents the strain responses during the cyclic CTE test. The local slopes of the loading-unloading cycles may present a resilient modulus measurement. Properties on compressibility, stress-path dependency of elastic moduli, creeping, accumulative plastic deformation, and dynamic modulus can be evaluated but are beyond the scope of this paper. This paper presents only the properties of anisotropic elasticity.

CONCLUSION

It is demonstrated in this paper that asphalt concrete under field compaction shows a general anisotropy that might be approximated as orthotropy. The anisotropy is quite significant. The

stress fields of an isotropic and an anisotropic pavement could be significantly different pending on the degree of the anisotropy measured by the ratios between the horizontal and vertical elasticity modulus. This significant difference has important implications to pavement design and analysis. Pavement design based on the isotropic elasticity analysis may underestimate the shear stress and tensile stress that are related to permanent deformation and fatigue cracking assessments. Multiple stage testing using the cubical cell device presents an effective tool for characterizing the properties and calibrating the constitutive models of asphalt concrete.

REFERENCES

[1] Kuwano, R; Connolly, TM; Jardine, RJ (2000). "Anisotropic Stiffness Measurements in A Stress-Path Triaxial Cell". Geotechnical Testing Journal, Vol.23, No.2, pp 141-157.

[2] Pennington, DS; Nash, DFT; Lings, ML (2001). **"**Horizontally Mounted Bender Elements for Measuring Anisotropic Shear Moduli in Triaxial Clay Specimens". Geotechnical Testing Journal, Vol. 24, No.2, pp 133-144.

[3] Adu-Osei, A; Little, DN; Lytton, RL (2001). **"**Cross-Anisotropic Characterization of Unbound Granular Materials". Transportation Research Record, No. 1757, pp 82-91.

[4] Roy, D; Campanella, RG; Byrne, PM; Hughes, J (2002). "Undrained Anisotropic Monotonic Behavior of Sand from In Situ Tests". Journal of Geotechnical and Geoenvironmental Engineering, Vol.128, No.1, pp 85-91.

[5] Li, XS; Dafalias, YF (2002). "Constitutive Modeling of Inherently Anisotropic Sand Behavior". Journal of Geotechnical and Geoenvironmental, Vol.128, No. 10 pp 868-880.

[6] Tutumluer, E; Adu-Osei, A; Little, DN; Lytton, RL (2001). **"**Field Validation of the Cross-Anisotropic Behavior of Unbound Aggregate Bases". ICAR-502-2.

[7] Seyhan, U; Tutumluer, E (2002). **"**Anisotropic Modular Ratios as Unbound Aggregate Performance Indicators". Journal of Materials in Civil Engineering,Vol.14, No.5, pp 409-416.

[8] Masad, E; Tashman, L; Somedavan, N; Little, D (2002). "Micromechanics-Based Analysis of Stiffness Anisotropy In Asphalt Mixtures". Journal of Materials in Civil Engineering, Vol.14, No.5, pp 374-383.

[9] Boulbibane, M; Weichert, D; Raad, L (1999). **"**Numerical Application of Shakedown Theory to Pavements with Anisotropic Layer Properties". Transportation Research Record, No.1687, pp 75-81.

[10] Wof, K. (1935). "Ausbreitung der Kraft in der Halbebene und im Halbraum bei anisotropem Material". Zeitschrift f. Angew. Math. Und Mech., B. 15, H.5.

[11] Hambley, E. C. (1969). "A New Triaxial Apparatus". Geotechnique, Vol. 19, No.2, pp. 307-309.

[12] Airey, D. W.; and Wood, D. M. (1988). "The Cambridge True Triaxial Apparatus". Advanced Triaxial Testing of Soil and Rock, STP 977, ASTM, Philadelphia, PA, pp. 796-805.

[13] Ko, H. Y.; and Scott, R. F. (1967). "A New Soil Testing Apparatus." Geotechnique, Vol.17, No.1, pp. 40-57.

[14] Sture, S.; and Desai, C. S. (1979). "A Fluid Cushion Truly Triaxial or Multiaxial Testing Device." ASTM Geotech. Test. J., Vol. 2, No.1, pp. 20-33.

[15] Green, G. E. (1971). "Strength and Deformation of Sand Measured in an Independent Stress Control Cell." Stress-Strain Behavior of Soils, Proc., Roscoe Memorial Symposium, G. T. Foulis and Co. Ltd., Cambridge, England, pp. 285-323.

[16] Lade, P. V.; and Duncan, J. M. (1973). "Cubical Triaxial Tests on Cohesionless Soil." ASCE J. Soil Mech, Found. Div., Vol. 99, SM10, pp. 793-812.

[17] Sture, S. (1979). "Development of Multiaxial Cubical Test Device With Pore-Water Pressure Monitoring Facilities." Report No. VPI-E-79.18, Dept. Civil Engrg., Virginia Polytechnic Institute and State University, Blacksburg, VA.

[18] Arthur, J. R. F. (1988). "Cubical Devices: Versatility and Constraints." Advanced Triaxial Testing of Soil and Rock, STP 977. ASTM, Philadelphia, PA, pp. 743-765.

[19] Atkinson, R. H. (1972). "A Cubical Test Cell For Multiaxial Testing of Materials." Ph.D. Dissertation, University of Colorado at Boulder, Boulder, CO.

[20] NeSmith, W. M. (1997). "Development of a Computer Controlled Multiaxial Cubical Testing Apparatus." M.Sc. Thesis, Georgia Institute of Technology, Atlanta, GA.

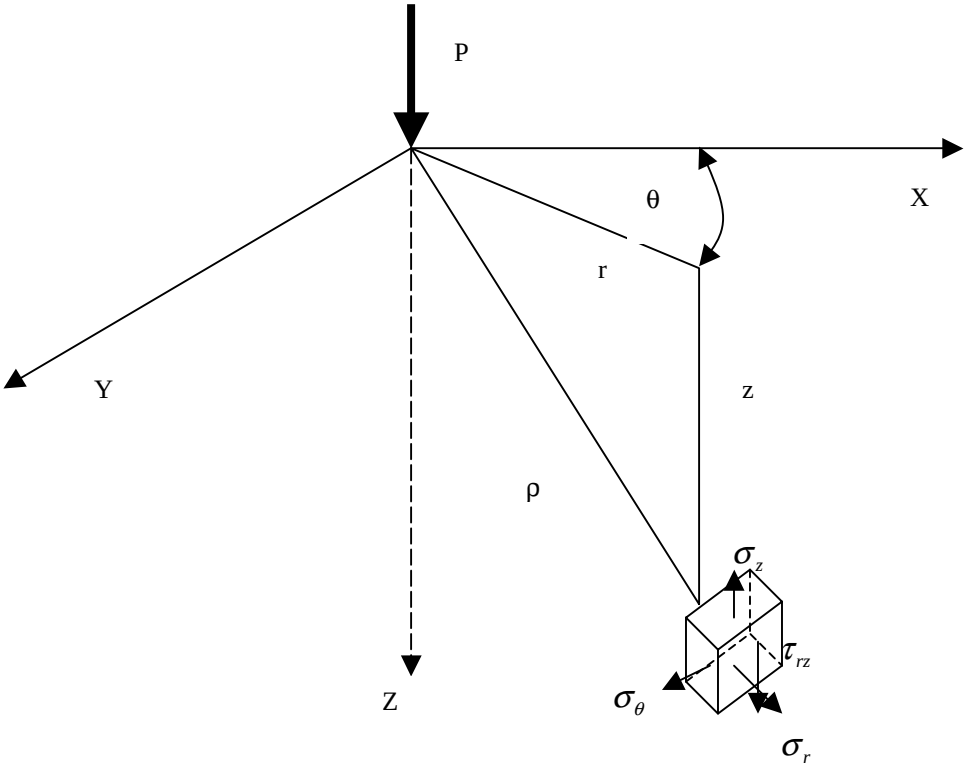

Figure 1. Illustration of the Geometric and Stress Terms

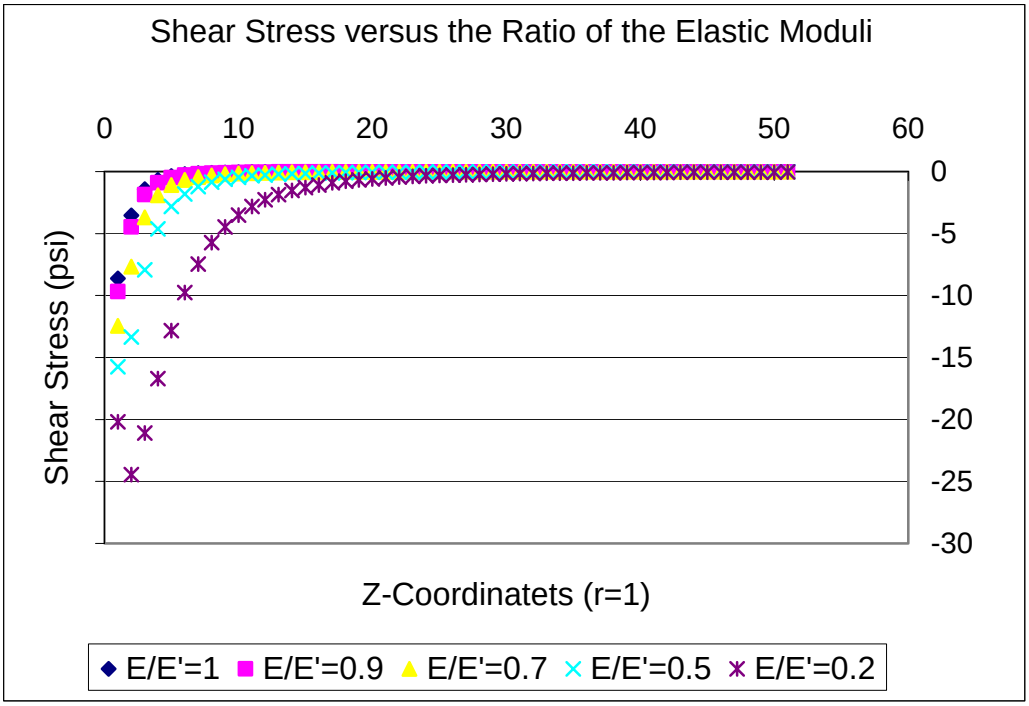

a. Shear Stress versus Elastic Modulus Ratio

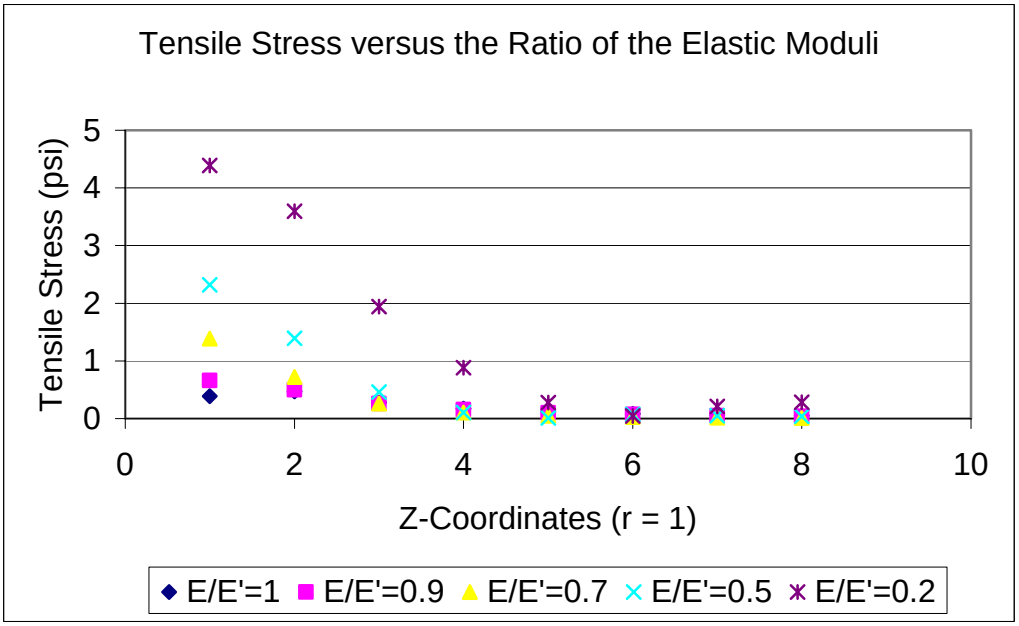

b. Tensile Stress versus Elastic Modulus Ratio
(Note, $E=E_h$ and $E'=E_v$)

Figure 2. Stress Distribution versus the Ratio of the Elastic Modulus

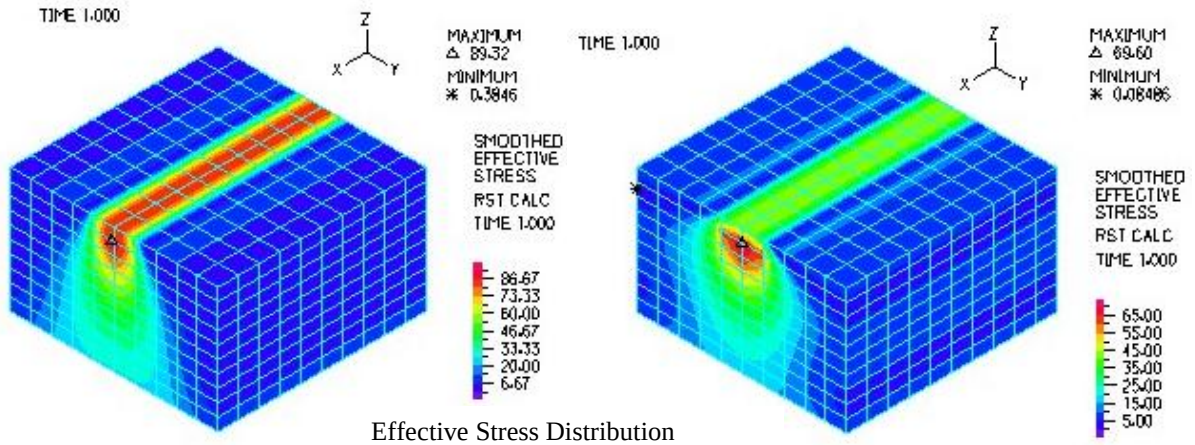

Effective Stress Distribution

$E_v=5E_h$ $E_v=E_h$

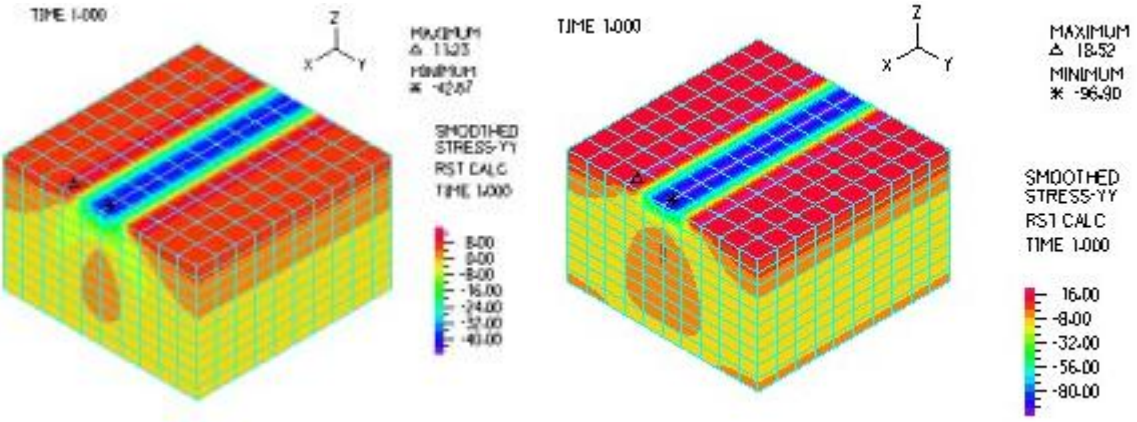

$E_v=5E_h$ Direct Stress in Y Direction $=E_h$

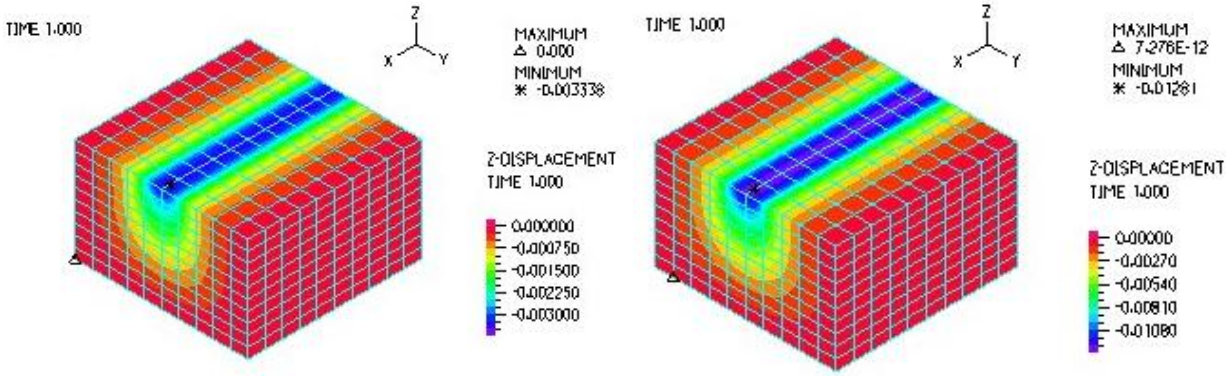

Vertical Displacement

$E_v=5E_h$ $E_v=E_h$

Figure 3. Typical Stress and Vertical Displacement Distribution for the Case of Fixed XYZ

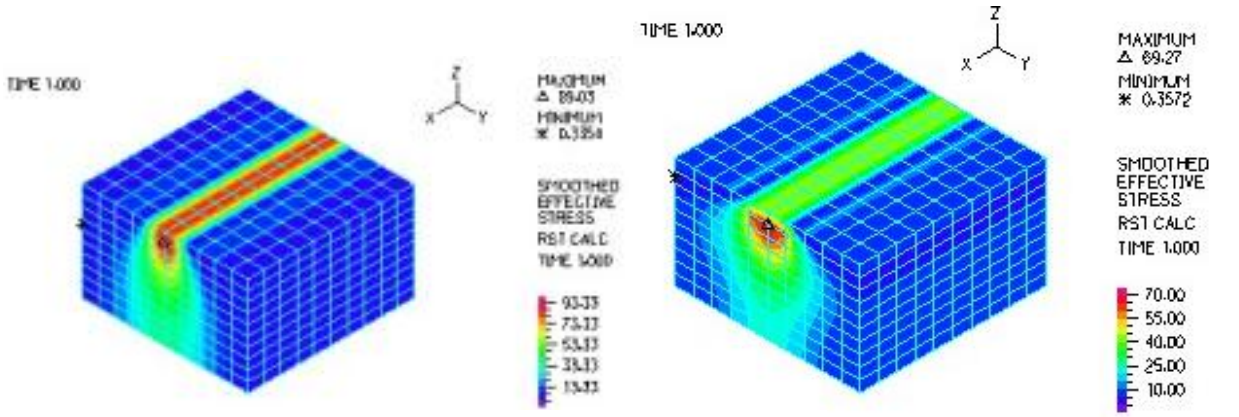

Effective Stress Distribution

$E_v=5E_h$ $E_v=E_h$

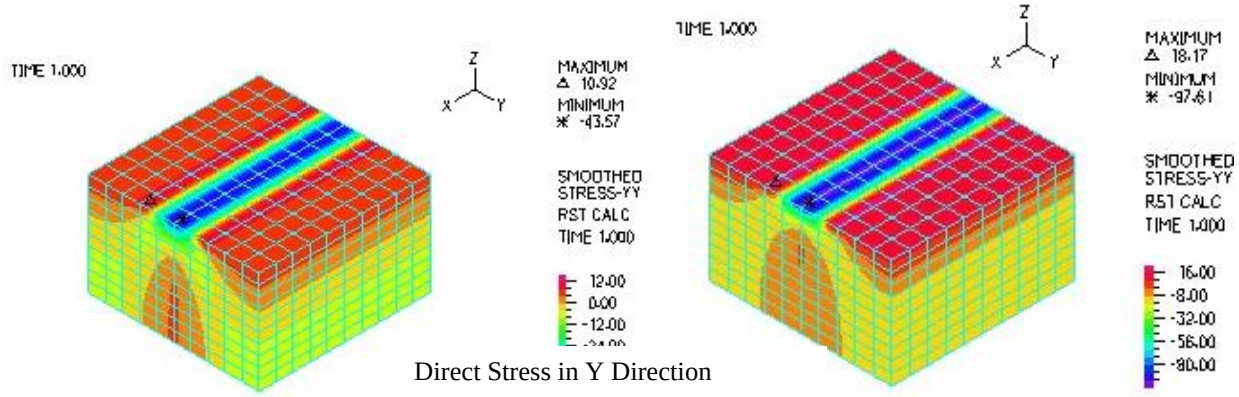

Direct Stress in Y Direction

$E_v=5E_h$ $E_v=E_h$

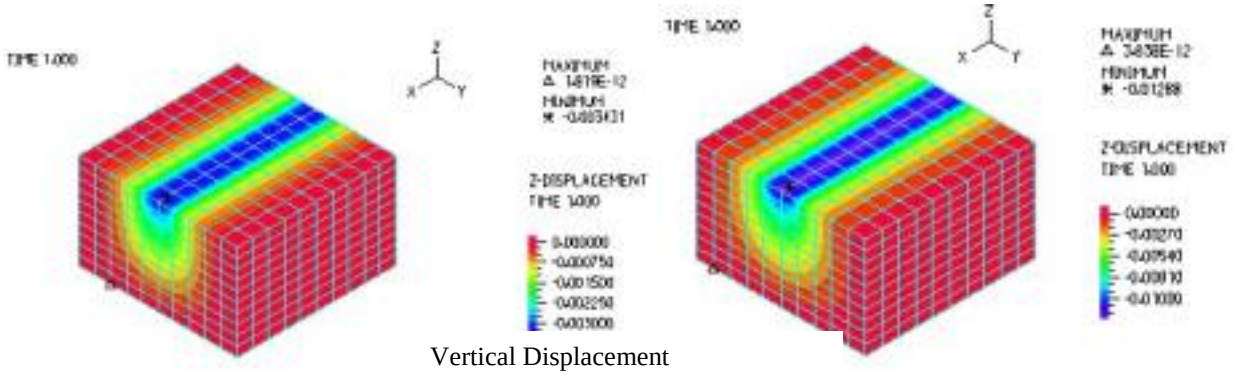

Vertical Displacement

$E_v=5E_h$ $E_v=E_h$

Figure 4. Typical Stress and Vertical Displacement Distribution for the Case of Fixed Z

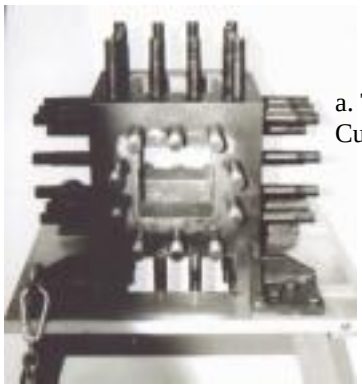

a. True Triaxial Cubical Frame

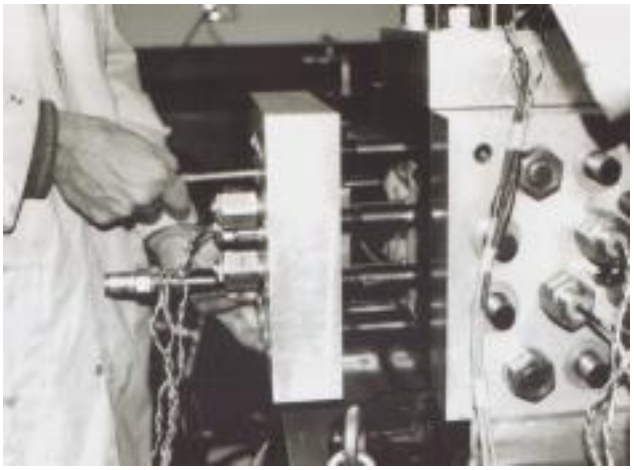

b. Lateral Walls

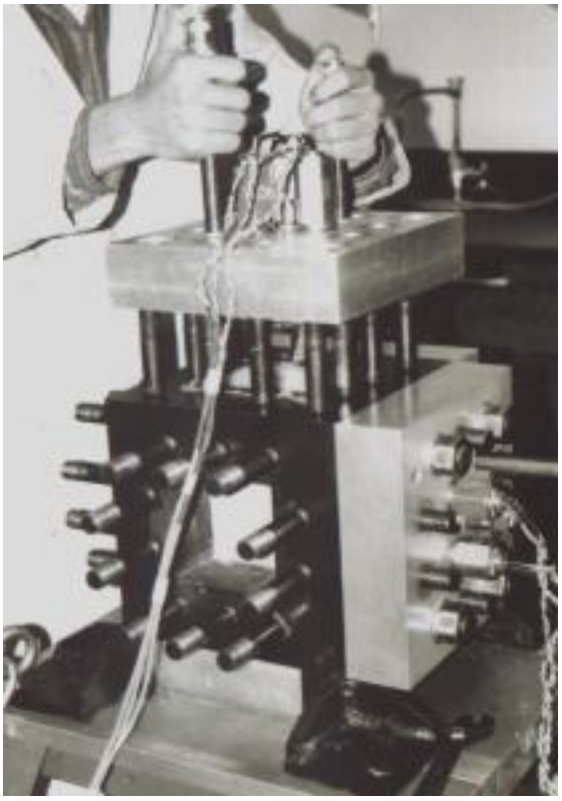

c. Top & Bottom Walls

Figure 5. Top, Bottom, and Lateral Wall Assemblies

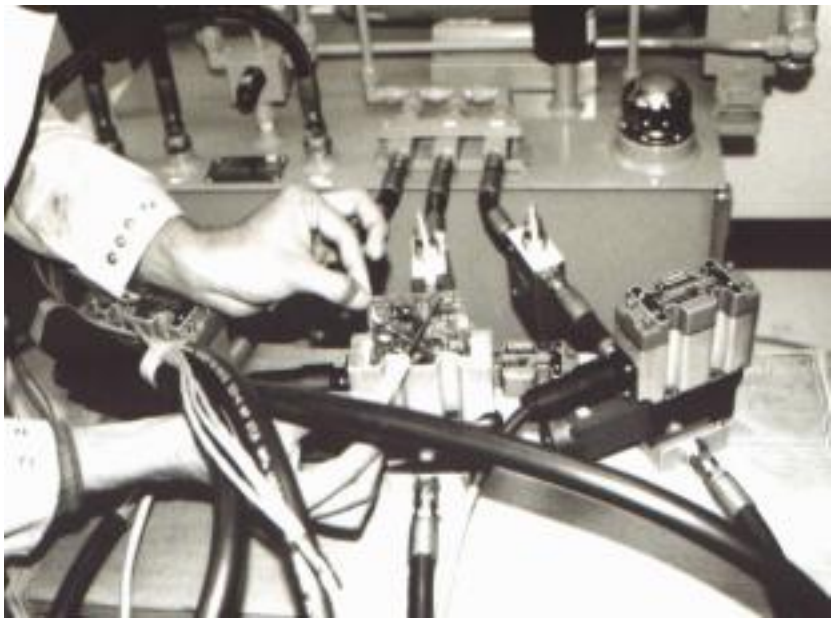

Figure 6. Calibration of Proportional Valves of Hydraulic Power Unit

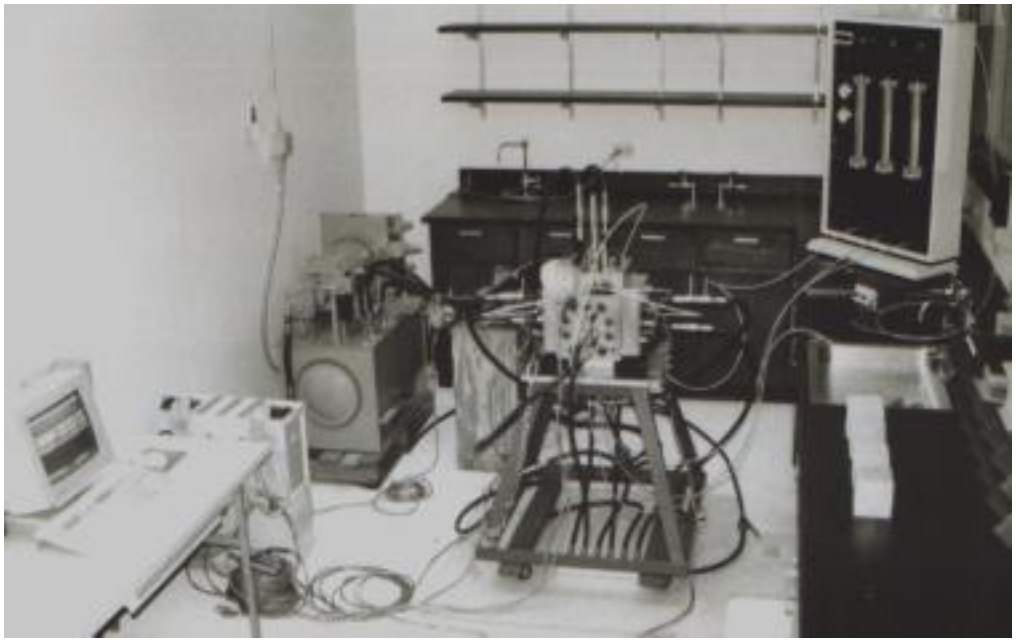

Figure 7. Overview of the Complete Testing Setup

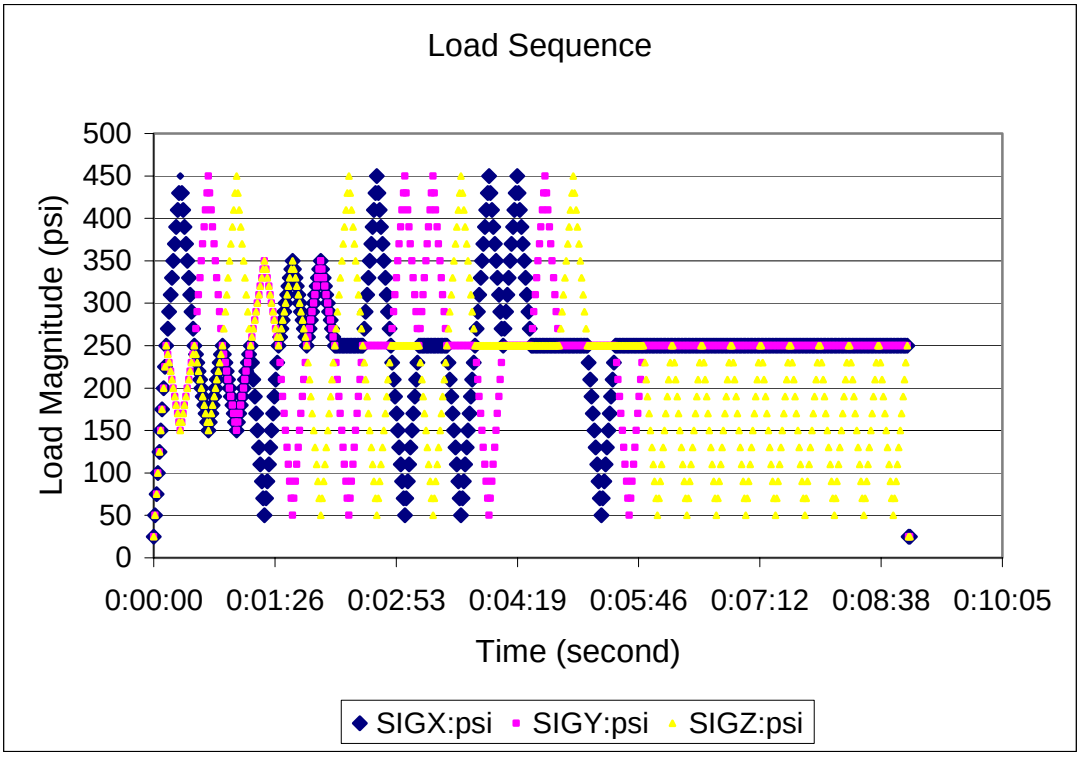

a. Load Sequence in the X, Y, and Z Space

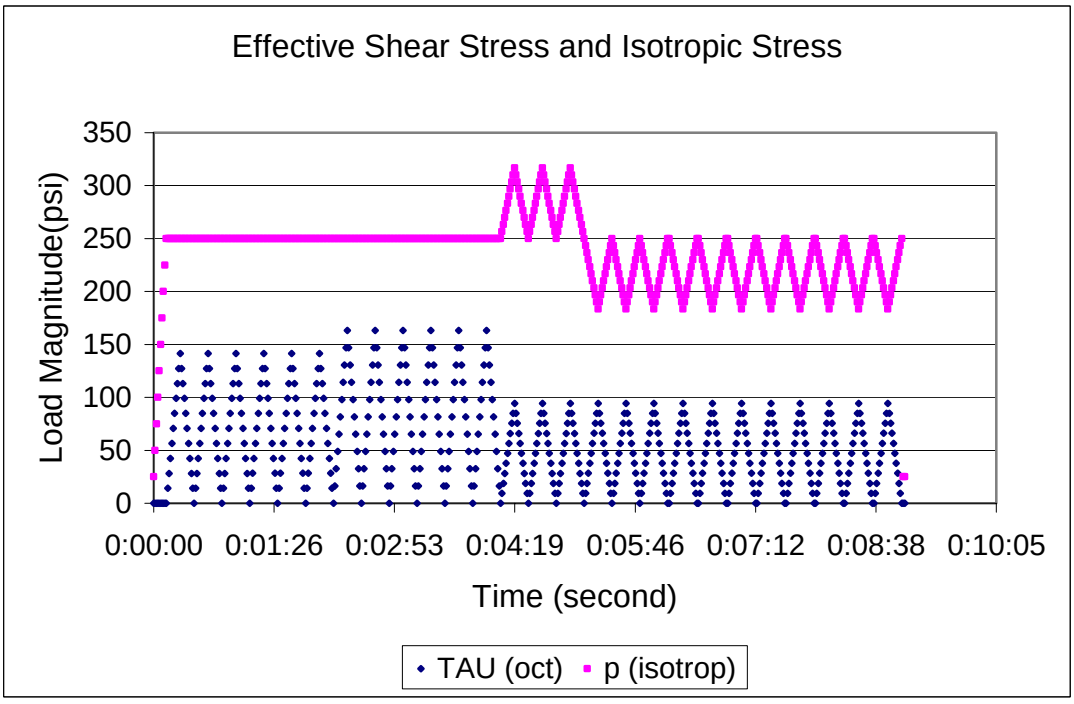

b. Load Sequence in the $\tau \sim p$ Space

Figure 8 Load Sequence of the Testing

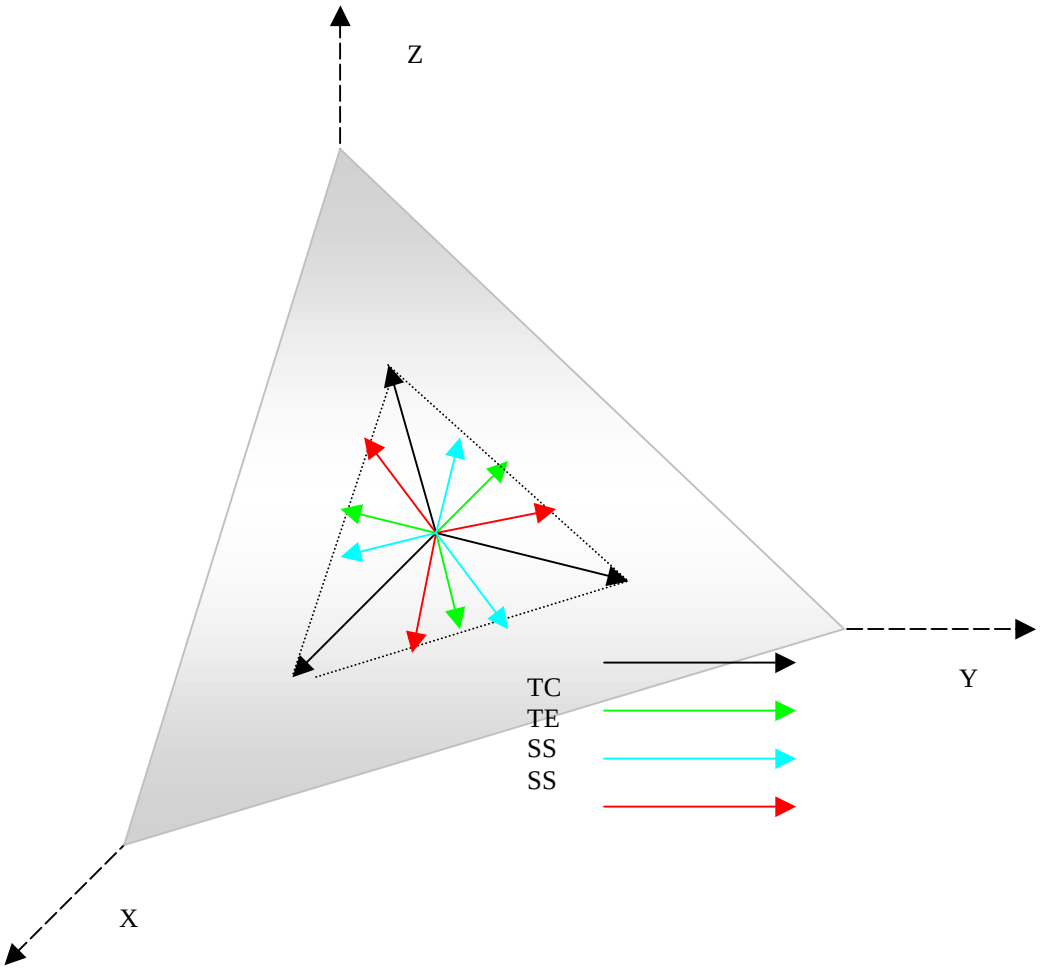

Figure 9. The TC, TE and SS Stress Paths on the π Plane

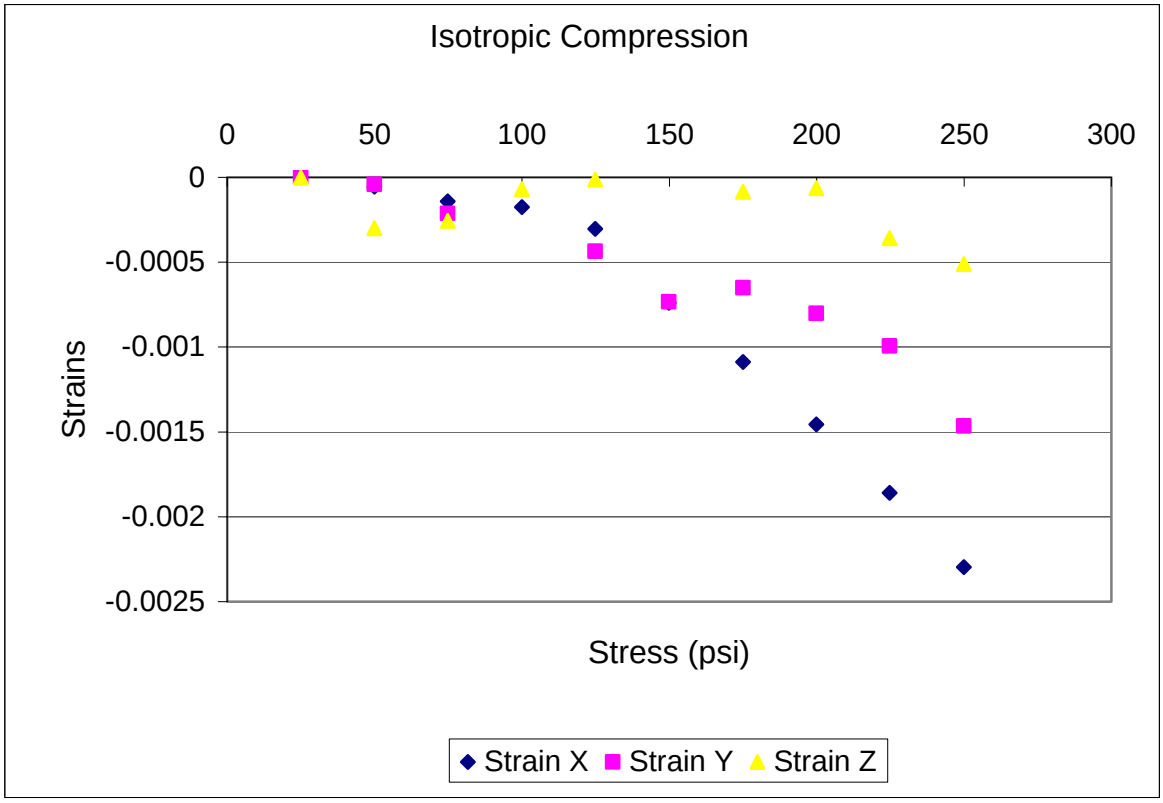

Figure 10. Stress-Strain Relation During Isotropic Compression

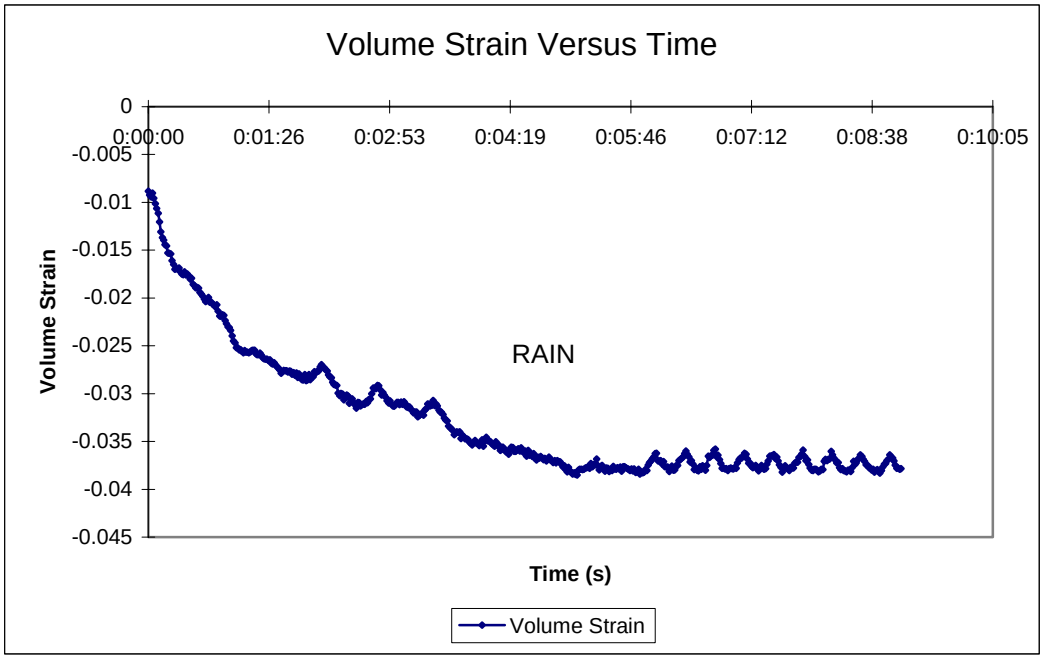

Figure 11 Volumetric Strain During the Entire Test

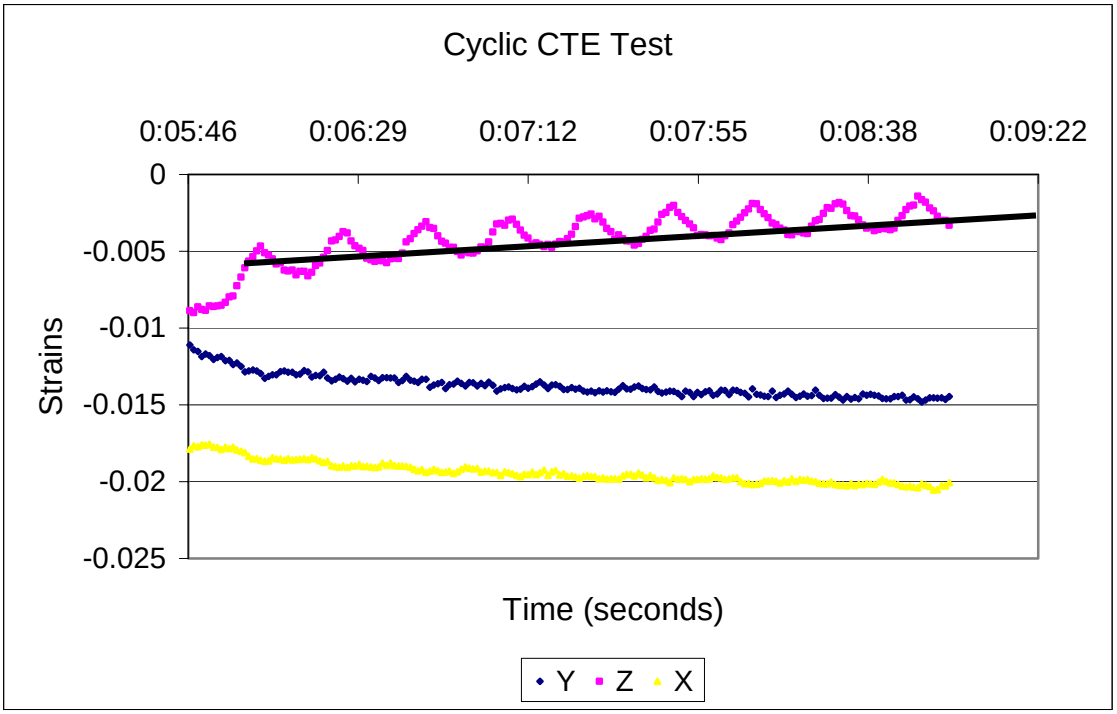

Figure 12 Strain Plot of the Cyclic CTE Test

Table 1 Material Properties for the Simulation

Case	Ev (Psi)	E_{hx} (Psi)	E_{hy} (Psi)	Poisson's Ratio	Shear Modulus G_x (Psi)	Shear Modulus G_y (Psi)	Shear Modulus G_z (Psi)
1	100000	100000	100000	0.3	3846.15	3846.15	38461.54
2	100000	80000	80000	0.3	3846.15	3846.15	30769.23
3	100000	50000	50000	0.3	3846.15	3846.15	19230.77
4	100000	20000	20000	0.3	3846.15	3846.15	7692.31
5	100000	10000	10000	0.3	3846.15	3846.15	3846.15

Note: Different expressions but are consistent with the orthotropic model.

Table 2 Test Sequence

Sequence No.	Test Designation	X	Y	Z
1	IC (to 250 psi)	↑	↑	↑
2	TC	↑	↓	↑
3	TC	↓	↑	↓
4	TC	↓	↓	↑
5	TE	↓	↑	↑
6	TE	↑	↓	↑
7	TE	↑	↑	↓
8	SS	Constant	↑	↓
9	SS	↑	Constant	↓
10	SS	↑	↓	Constant
11	SS	Constant	↓	↑
12	SS	↓	Constant	↑
13	SS	↓	↑	Constant
14	CTC	↑	Constant	Constant
15	CTC	Constant	↑	Constant
16	CTC	Constant	Constant	↑
17	CTE	↓	Constant	Constant
18	CTE	Constant	↓	Constant
19	CTE	Constant	Constant	↓
20	CCTE	Constant	Constant	↓↑

↑ Stress increase
↑ Stress decrease